A machine learning method to evaluate head sea induced weather impact on ship fuel consumption

Citation for the original published paper (version of record):
Zhang, C., Vergara, D., Zhang, M. et al (2025). A machine learning method to evaluate head sea induced weather impact on ship fuel consumption. Energy, 328.
http://dx.doi.org/10.1016/j.energy.2025.136533

(article starts on next page)

Energy 328 (2025) 136533

Contents lists available at ScienceDirect

Energy

journal homepage: www.elsevier.com/locate/energy

A machine learning method to evaluate head sea induced weather impact on ship fuel consumption

Chi Zhang [a], Daniel Vergara [a], Mingyang Zhang [b], Tsoulakos Nikolaos [c], Wengang Mao [a,*]

[a] Department of Mechanics and Maritime Sciences, Chalmers University of Technology, Sweden
[b] Department of Mechanical Engineering, Aalto University, Finland
[c] Laskaridis Shipping Company Co. Ltd., Kifissia, Athens, Greece

ARTICLE INFO

Handling Editor: Prof X Ou

Keywords:
Added wave resistance
Head wave
Gaussian process regression
Machine learning
Ship fuel consumption
Weather impact

ABSTRACT

A ship's fuel consumption is significantly affected due to ship motions caused by waves and wind when sailing under ocean weather conditions. An essential step to develop certain energy efficiency measures is to understand, model and estimate how much extra fuel consumption is caused by encountering weather conditions, and from which components of a ship's energy system that extra consumption is attributed to. In this study, experimental tests of added resistance in waves during the past decades in open literature are collected and a Gaussian process regression (GPR) model is developed to describe a generic ship's added resistance in head waves. The proposed GPR model achieves better prediction accuracy than semi-empirical formulas (white box) and gives more rational transfer function of added wave resistance coefficient than those produced by the artificial neural networks (ANN), especially in the short-wave regime. The proposed GPR model is integrated into a grey box prediction framework for ship fuel consumption using several years of performance monitoring data collected onboard a chemical tanker. The prediction results indicate an improvement in model performance when moving from the white box to the grey box model, with R^2 increasing by 38 % and Root Mean Square Error (RMSE) decreasing by 65 %. Finally, the investigation of weather impact on the ship's extra fuel cost is demonstrated by the proposed model.

1. Introduction

The International Maritime Organization (IMO) adopted its updated GHG strategy to significantly reduce GHG emissions from ships [1]. The new targets were set to reduce 20 % by 2030, 70 % by 2040, and achieve zero emissions by 2050. The technical indicator, i.e., Energy Efficiency Existing Ship Index (EEXI) [2], and the operational indicator, i.e., Carbon Intensity Indicator (CII) [2], were introduced to monitor the decarbonization process in the shipping industry. Before the supply of zero-emission fuel is fully available for the shipping market by 2050 [3], market uptakes of measures to increase shipping energy efficiency are essential to fulfil the intermediate IMO emission goals [1]. Since most of a ship's service time is sailing at sea, the weather conditions contribute to about 15 % of a ship's total fuel consumption [4]. Furthermore, for the better development, installation, and evaluation of energy efficiency measures [5], it is essential to understand and model how the encountered sea environments affect different energy system components [4]. These effects, often referred to as the "weather impact", include added resistance, varying propulsion efficiency, and involuntary speed reductions, all of which influence the values of CII and EEXI [6]. One challenging task to evaluate a ship's weather impact is accurate modelling and estimating added resistance in waves, which causes additional fuel consumption [7]. Various models/methods are available for such estimation, such as experimental model tests, computational fluid dynamics (CFD) and potential-flow based numerical analysis [8–11]. Tank model tests are often regarded as the most reliable prediction method for added resistance, but they are very expensive in terms of test facilities and personnel costs. High-fidelity CFD simulations may provide reliable results but are time-consuming and computationally intensive. Lee et al. [12] employed CFD simulations to analyze diffraction-induced added resistance and wake characteristics in head waves for two ship types. Potential flow methods are often used to evaluate added wave resistance. For example, Kim and Kim [8] utilized a higher-order Rankine panel method to predict added resistance on ships in irregular waves. Kim et al. [13] conducted experimental and numerical investigations using potential flow and CFD methods to evaluate

* Corresponding author.
E-mail address: wengang.mao@chalmers.se (W. Mao).

https://doi.org/10.1016/j.energy.2025.136533
Received 21 March 2025; Received in revised form 26 April 2025; Accepted 9 May 2025
Available online 12 May 2025

the motions and added resistance of an LNG carrier in oblique waves. Chen et al. [14] applied the Taylor Expansion Boundary Element Method to solve 3D unsteady potential flow for ships in waves to predict wave forces. However, these methods are still time-consuming and require comprehensive data of hull geometry.

Alternatively, empirical or semi-empirical formulations are often used for fast prediction of added resistance in waves for the ship design purpose [11], which recommends an integration method to estimate a ship's added resistance in waves based on the empirical formulas to describe the added wave resistance transfer function, i.e., wave resistance under a series of wave frequencies. Fujii and Takahashi [15] was the first to introduce the semi-empirical formulas to account for the added resistance caused by wave reflection. Liu and Papanikolaou [10, 16] improved existing formulas by adding correction terms for ship characteristics such as waterline entrance angle and block coefficient various ship types. Lang and Mao [17] proposed a semi-empirical model for predicting add wave resistance. They introduced a correction factor for significant wave height to account for high wave impacts due to nonlinear ship motions at rough sea environments. The parameters within those empirical formulas were often derived from many model tests by some least square. However, obvious discrepancies cannot be avoided due to the characters of least square used in the empirical formulas.

For the past few years, artificial neural networks (ANNs) have been utilized for estimating added resistance. These models offer computational efficiency and accuracy [18,19]. ANNs perform fast predictions through simple nonlinear operations at each neuron, fitting any function by combining a large number of neurons. Cepowski [18] investigated the application of two-layer ANN to predict added resistance in regular head waves, using ship design parameters like length, breadth, draught, and Froude number. The developed ANN was trained based on published experimental data and presented as a mathematical function. Cepowski [20] further advanced this research by developing a set of five ANNs trained on fundamental design parameters. Results indicated that using a set of five ANNs provided more accurate estimates than a single ANN. Duan et al. [19] proposed a method using deep feedforward neural networks (DFNs) with optimized activation function for fast prediction of added resistance in heading waves. They addressed the complexity of semi-empirical formulas and the limitations of single hidden layer neural networks. Sun et al. [21] designed an ANN to estimate ship resistance in ice-covered waters. The Radial Basis Function - Particle Swarm Optimization (RBF-PSO) algorithm with seven features was found to set as input variables. While the above ANN based methods treated each test, i.e., wave resistance at each individual wave frequency as an independent sample/inputs, the correlation of added wave resistance under a series of wave frequency for the same speed should be reflected.

In this study, we developed a Gaussian process regression (GPR) model to predict the added wave resistance for ships. Like the approaches by Cepowski [20] and Duan et al. [19], our data comes from experimental tests published in open literature. These experimental datasets are organized according to individual experiments. Thus, in each experimental dataset, the data points have high correlations with each other. This GPR-based approach is motivated by the need to effectively capture these correlations through kernel functions, improving the model's predictive performance [22]. Additionally, the inputs of the GPR model are expanded to include more ship geometry features. To ensure robust validation, we defined several data partitioning strategies for model's training and test. The proposed GPR model is subsequently integrated into a grey box prediction framework for ship fuel consumption using several years of performance monitoring data collected onboard a chemical tanker. The workflow of this paper is shown in Fig. 1.

The rest of the article is organized as follows. Section 2 introduces the method to evaluate fuel consumption due to weather impact, and different models for predicting added wave resistance. The dataset used for training the model is described in Sections 3. The results of wave resistance prediction are presented in Section 4. In Section 5, the application of proposed method is proposed for ship performance prediction, and a grey box model is proposed for ship fuel consumption prediction and weather impact analysis.

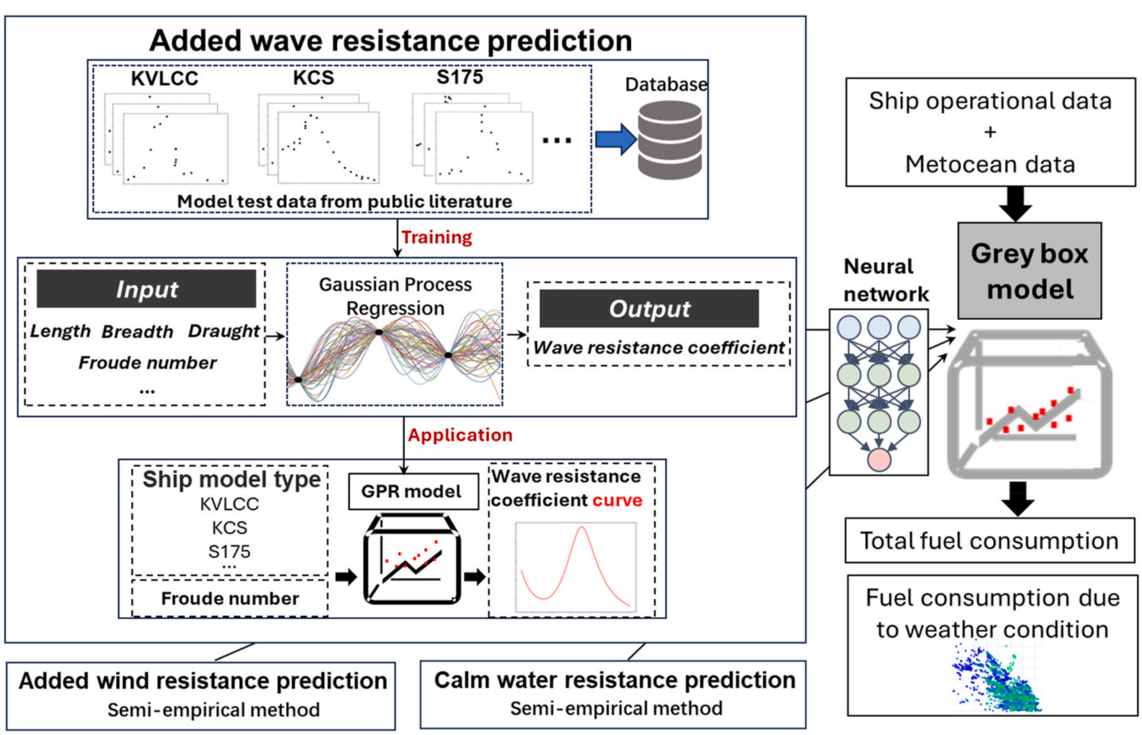

Fig. 1. Workflow of this paper.

2. Ship technical and operational indicators

During navigation, the ship's propulsion system provides power while the ship encounters resistance from the environment. In addition to wave resistance, the ship also experiences calm water resistance, wind resistance, and other forms of resistance, as shown in Fig. 2.

2.1. Problem formulation of weather influence factor f_w

Ship fuel consumption during navigation FC can be considered as consisting of calm water resistance FC_{calm}, wind resistance FC_{wind}, and wave resistance FC_{wave}. The sum of the latter two can be considered as fuel consumption due to weather conditions $FC_{weather}$:

$$FC = FC_{calm} + (FC_{wave} + FC_{wind}) = FC_{calm} + FC_{weather} \tag{1}$$

Now we can define weather influence factor f_w:

$$f_w = \frac{FC_{weather}}{FC} \tag{2}$$

To get a good estimation of such f_w, calm water resistance and added resistance due to wind and waves are needed to be estimated. We define $\boldsymbol{W} = [H_s, T_z, \theta, V_{wr}, \psi]$ to describe weather conditions, where H_s is the significant wave height; T_z is the mean wave period; θ is the mean wave direction; V_{wr} is the relative wind speed; ψ is the relative wind direction. The fuel consumption under the weather condition of $\boldsymbol{W}$ and ship speed V is estimated by:

$$FC(V,\boldsymbol{W}) = \frac{P_e(V,\boldsymbol{W})}{\eta} \times SFOC = \frac{(R_{calm}(V) + R_{weather}(V,\boldsymbol{W})) \times V}{\eta} \times SFOC \tag{3}$$

where $SFOC$ is the specific fuel consumption, η represents the power transition coefficient, which is a composite coefficient derived from the product of various efficiencies, including shaft transmission efficiency, rotative efficiency, open water propeller efficiency, and ship hull efficiency. The calm water resistance primarily consists of frictional resistance caused by the viscosity of the water and wave-making resistance due to pressure changes around the hull. According to the semi-empirical formula recommended by the ITTC [23], the calculation formula for still water resistance is as follows:

$$R_{calm} = \frac{1}{2} C_f \rho_w S V_{cw}{}^2 \tag{4}$$

where C_f represents the calm water resistance coefficient of a specific vessel from towing tank tests; ρ_w denotes the density of seawater; S is the wetted surface area; and V_{cw} is the calm water speed.

2.1.1. Added resistance due to wind

The resistance increase due to the wind effect on the ship above waterline and superstructure, is predicted using formula Eq. (5), given by the International Organization for Standardization [24]:

$$R_{AA} = \frac{1}{2}\rho_A \left[C_A(\psi) A_{XV} V_{wr}{}^2 - C_A(0) A_{XV} V_G{}^2\right] \tag{5}$$

where ρ_A represents the air density; A_{XV} denotes the projected area of the portion of the hull above the waterline on the transverse section; V_{wr} is the relative wind speed, ψ indicates the angle between the wind direction and the ship's heading, and V_G is the ship's speed. The wind resistance coefficient C_A measured through wind tunnel tests is given by shipowners for this study. The above added wind resistance is relatively easier to estimate in comparison with the added wave resistance. In the following, different ways to estimate the added resistance due to wave will be presented, as well as the one proposed by this study.

2.2. Added resistance due to wave

In Liu and Papanikolaou (2016), a fast estimation method of added resistance due to wave is introduced and compared to model tests, with a good agreement. The actual sea state experienced by a ship during navigation consists of irregular waves, which can be considered as a superposition of a series of regular waves with frequencies ω. Therefore, the average resistance of a ship in irregular waves ($\overline{R}_{aw}$) can be estimated by integrating the transfer function of added resistance in regular waves (R_{aw}) with the wave spectrum $S(\omega)$. The transfer function of added resistance in regular waves at different speeds can be obtained using different methods (such as semi-empirical formulas, black-box models, and CFD). The wave spectrum $S(\omega)$ is characterized by the significant wave height (H_s) and the characteristic wave period (T), which describe the actual sea conditions. The total added resistance in irregular waves due to wave spectrum $S(\omega)$ can be computed by the linear integration of the resistances from its regular wave components as shown:

$$\overline{R}_{aw}(V,\boldsymbol{W}) = 2\int_0^\infty S(\omega|\boldsymbol{W}) \frac{R_{aw}(w|V,\boldsymbol{W})}{\zeta_a(\omega)^2} d\omega \tag{6}$$

$$C_{aw}(w|V,\boldsymbol{W}) = \frac{R_{aw}(w|V,\boldsymbol{W})}{\rho_w g \zeta_a^2 B^2/L} \tag{7}$$

Where C_{aw} is the nondimensional transfer function of added wave resistance in regular waves; B is the breadth of the ship; ζ_a is the wave amplitude. In this study, the JONSWAP wave spectrum is employed for the calculations, and it is defined as follows:

$$S(\omega) = \frac{320 H_s{}^2}{T_p^4 \omega^5} exp\left(\frac{-1950}{T_p^4 \omega^4}\right) \gamma^{exp\left[\frac{-(\omega-\omega_p)^2}{2\sigma^2\omega_p^2}\right]} \tag{8}$$

where H_s is the significant wave height; T_p is wave peak period; γ is extra peak enhancement factor; ω_p is spectral peak frequency; σ is spectral width parameter.

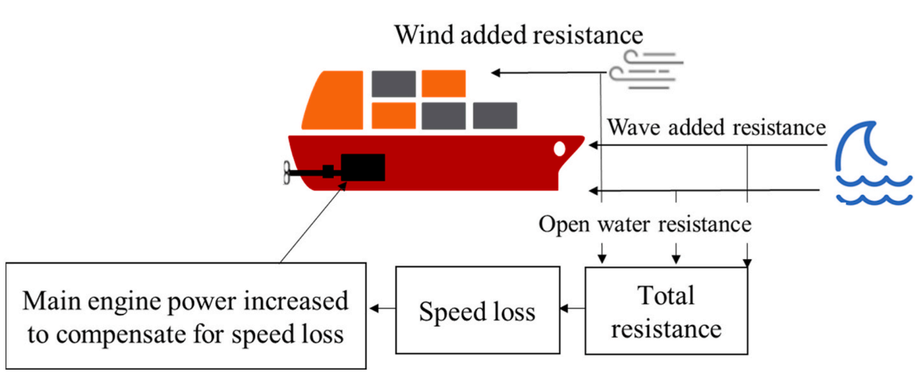

Fig. 2. Resistance component for ship navigation.

2.2.1. Semi-empirical models for C_{aw} transfer function

The changing of added wave resistance on a ship depends on factors, including hull geometry, operating conditions, and wave characteristics. Regarding the nondimensional transfer function for mean resistance in regular waves, its primary determinants are wave frequency, heading, and speed. Thus, different methods' performance for predicting C_{aw} are usually assessed by grouping the prediction according to Froude number and wavelength ratio for different ship types. For developing semi-empirical models, Liu and Papanikolaou [10] initially introduced a statistical approach that merges Faltinsen [25] with Jinkine and Ferdinande [26]. In their subsequent studies [16], they incorporated heading-based trigonometric functions into the original formulation and broadened its applicability to shallow draft, ballast conditions, and arbitrary wave scenarios through regression analysis on extensive experimental data. Meanwhile, Lang and Mao [17] proposed an added wave resistance model for head seas, drawing on Tsujimoto et al. [27] as well as Jinkine and Ferdinande [26]. Their model was influenced by equations presented by Liu and Papanikolaou [10], and certain calculations were refined using relevant experimental datasets. Later, this model was updated to account for arbitrary waves by incorporating an encountered-frequency correction factor [28]. For detailed formulas and application guidelines, see the original publications [16,17].

2.2.2. Data-driven models for C_{aw} transfer function and architecture of GPR model

Unlike semi-empirical formulas, data-driven models rely entirely on data to modelling. For added wave resistance coefficient prediction, all data-driven approaches reported to date in this field have been based on neural networks [18–20]. The choice of input variables is more flexible and driven by the available dataset; nonetheless, nearly all models incorporate the Froude number and the principal geometric parameters (length, beam, and draft) as inputs.

In this study, we develop a GPR model to predict additional wave resistance for ships. The experimental data derived from public literature is organized according to individual experiments, resulting in high correlations within each dataset. Through the implementation of this approach, the correlations within the dataset can be effectively captured for better model performance. The input and output variables are shown in Table 1.

In Table 1, L_E is length of entrance. L_E is described as the horizontal distance from the point where the waterline surface length attains 99 % of the ship's breadth to the Forepeak, which is considered as an important parameter for wave resistance prediction in semi-empirical formulas developed by Liu and Papanikolaou (2019), and Lang and Mao [17], as shown in Fig. 3. The variables in GPR model are all dimensionless, which is necessary because the numerical range of different input parameters varies significantly. For example, ship length L values range from 121 to 325, while F_n values are between 0 and 0.5. If left unaddressed, this issue could result in the model failing to learn input information with smaller numerical values.

Gaussian process regression is a non-parametric Bayesian approach to regression problems [22], which can provide probabilistic predictions along with uncertainty estimates. A GPR model can be defined as follows with an i-th input $\boldsymbol{x}_i$:

Table 1
Input and output variables in the GPR model for C_{aw} prediction.

	Description	Attributes
Input	Wavelength-to-ship length ratio	λ/L
	Froude number	F_n
	Block coefficient	C_B
	Beam-to-draft ratio	B/T
	Non-dimensional radius of gyration in yaw	K_{yy}/L
	Effective ship length ratio	L_E/L
Output	Added wave resistance coefficient	C_{aw}

$$C_{aw}^{i} = f(\boldsymbol{x}_i) + \varepsilon_i \tag{9}$$

where $\varepsilon_i \sim \mathcal{N}(0, \sigma_n^2)$, σ_n^2 is the noise variance. The unknown latent function $f(\cdot)$ is assumed Gaussian process prior where $f(\cdot) \sim \mathcal{GP}(\mu(\cdot), k(\cdot))$. $\mu(\cdot)$ refers to the mean function, which is usually set to zero for simplicity, and $k(\cdot)$ is the covariance (kernel) function. All the input variables in the training data set are denoted as:

$$\boldsymbol{X} = \{\boldsymbol{x}_i, i = 1, \ldots, n\} \tag{10}$$

$$\mathbf{f} = [\mathrm{f}_1, \mathrm{f}_2, \mathrm{f}_3, \ldots, \mathrm{f}_n]^T = [f(\boldsymbol{x}_1), f(\boldsymbol{x}_2), f(\boldsymbol{x}_3), \ldots, f(\boldsymbol{x}_n)]^T \tag{11}$$

where $\mathbf{f} \sim \mathcal{N}(\boldsymbol{\mu}(\boldsymbol{X}), \boldsymbol{K}(\boldsymbol{X}, \boldsymbol{X}))$. All the values of C_{aw} in the data set can be defined as:

$$\boldsymbol{C_{aw}} = \{C_{aw}^{i}, i = 1, \ldots, n\} \tag{12}$$

$$\boldsymbol{C_{aw}} \sim \mathcal{N}(\boldsymbol{\mu}(\boldsymbol{X}), \boldsymbol{K}(\boldsymbol{X}, \boldsymbol{X}) + \sigma_n^2 \boldsymbol{I}) \tag{13}$$

where $\boldsymbol{C_{aw}}$ is joint Gaussian distributed, i.e., and $\boldsymbol{I}$ is an identity matrix.

For a new input $\boldsymbol{x}_*$ to be predicted, a prior assumption is that there exists the same Gaussian distribution, and $\boldsymbol{C_{aw}}$ and $f(\boldsymbol{x}_*)$ follow the joint Gaussian prior distribution:

$$\begin{bmatrix} \boldsymbol{C_{aw}} \\ \mathrm{f}_* \end{bmatrix} \sim \mathcal{N}\left(\begin{pmatrix} \boldsymbol{\mu}(\boldsymbol{X}) \\ \mu(\boldsymbol{x}_*) \end{pmatrix}, \begin{pmatrix} \boldsymbol{K}(\boldsymbol{X}, \boldsymbol{X}) + \sigma_n^2 \boldsymbol{I} & \boldsymbol{K}(\boldsymbol{X}, \boldsymbol{x}_*) \\ \boldsymbol{K}(\boldsymbol{x}_*, \boldsymbol{X}) & k(\boldsymbol{x}_*, \boldsymbol{x}_*) \end{pmatrix} \right) \tag{14}$$

In a Bayesian framework, the key equation of GPR is the conditional distribution given the observed data samples, described as:

$$\mathrm{f}_* | \boldsymbol{X}, \boldsymbol{C_{aw}}, \boldsymbol{x}_* \sim \mathcal{N}(\bar{\mathrm{f}}_*, \Sigma_{\mathrm{f}_*}) \tag{15}$$

where:

$$\bar{\mathrm{f}}_* = \boldsymbol{K}(\boldsymbol{x}_*, \boldsymbol{X}) [\boldsymbol{K}(\boldsymbol{X}, \boldsymbol{X}) + \sigma_n^2 \boldsymbol{I}]^{-1} \boldsymbol{C_{aw}} \tag{16}$$

$$\mathrm{Var}\,(\mathrm{f}_*) = k(\boldsymbol{x}_*, \boldsymbol{x}_*) - \boldsymbol{K}(\boldsymbol{x}_*, \boldsymbol{X}) \, [\boldsymbol{K}(\boldsymbol{X}, \boldsymbol{X}) + \sigma_n^2 \boldsymbol{I}]^{-1} \boldsymbol{K}(\boldsymbol{X}, \boldsymbol{x}_*) \tag{17}$$

where $\bar{\mathrm{f}}_*$ is the predicted mean value of wave resistance coefficient based on input $\boldsymbol{x}_*$, and Var (f_*) is the variance to incorporate the uncertainty into the predictions. Using the above method, the mean value $\bar{\mathrm{f}}_*$ and variance Var (f_*) of wave resistance coefficient for different ship types under various speed and wavelength can be predicted.

3. Estimation of various models for C_{aw}

In this study, the list of ship particulars with experimental tests used here is shown in Table 2.

3.1. Experimental database for modelling

In this context, [λ/L, F_n, C_B, B/T, L/B, K_{yy}/L, L_E/L] serve as model inputs, while the output is the non-dimensional wave added resistance, represented as C_{aw}. The datasets used for predicting added wave resistance in head seas comprise model experimental data from published studies. This dataset comprises 2096 samples from approximately 45 ships and 175 distinct experimental cases. Fig. 4 illustrates the distribution of these parameters for the ships used in the study.

For example, the datasets collected from Chen et al. [29], Lee et al. [30] and Park et al. [31] are shown in Fig. 5. Data points from different experiments can be regarded as independent. But they will be highly correlated if coming from the same test, revealing a distinct trend of C_{aw} changing with λ/L.

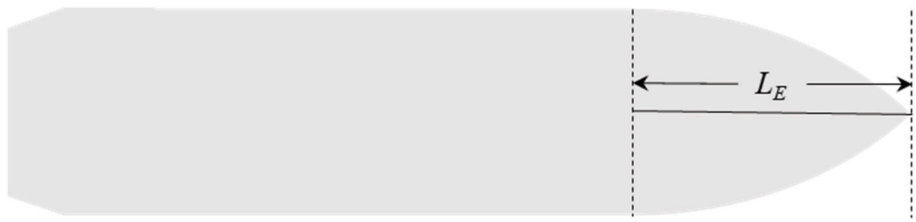

Fig. 3. Definition of L_E.

Table 2
Main parameters of the studied ships.

Ship type	L (m)	B (m)	T (m)	C_B
KVLCC	320	58	20.8	0.81
S175	175	25.4	9.5	0.57
KCS	230	32.2	10.8	0.65
Hull 2020	187.3	32.28	12	0.82
JBC	280	45	16.5	0.86
SR108	3.5	0.508	0.19	0.57
Aframax	248	43	14.3	0.84
SCb87	178	32.26	14.46	0.87
Supramax	192	36	11.2	0.81

3.2. Different strategies of splitting data for model training

The entire input set is a matrix with dimensions of 7 × 2096. To investigate the potential of different models, we designed two data partitioning strategies, as shown in Fig. 6:

- Strategy 1: The entire dataset is randomly shuffled, and then 10 % of the data is randomly selected to form the test set.
- Strategy 2: Entire sets of experimental data for different ship types (e.g., KVLCC, S175 and Hull 2020, etc.) are randomly selected to form the test set, comprising approximately 10 % of the total dataset, which means a complete set of experimental data for any ship type might be included in the test set. The main parameters of these ship types, such as length, breadth, draft, and block coefficient, are listed in Table 2. This strategy allows for a focused evaluation of the model's performance on ship types.

To measure the accuracy of the predictive models, the Root Mean Square Error (RMSE) and R^2 are employed to assess their performance:

$$\mathrm{RMSE} = \sqrt{\frac{\sum_{i=1}^{n}(p_i - a_i)^2}{n}} \tag{19}$$

$$R^2 = 1 - \frac{\sum_{i=1}^{n}(p_i - a_i)^2}{\sum_{i=1}^{n}(a_i - \overline{a})^2} \tag{20}$$

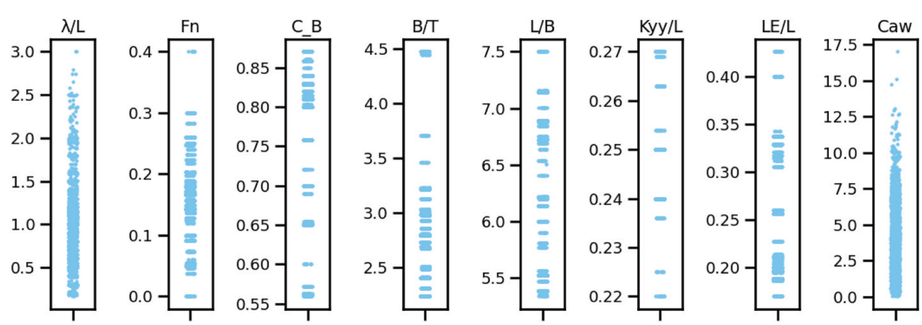

Fig. 4. The distribution of input and output parameters in the datasets.

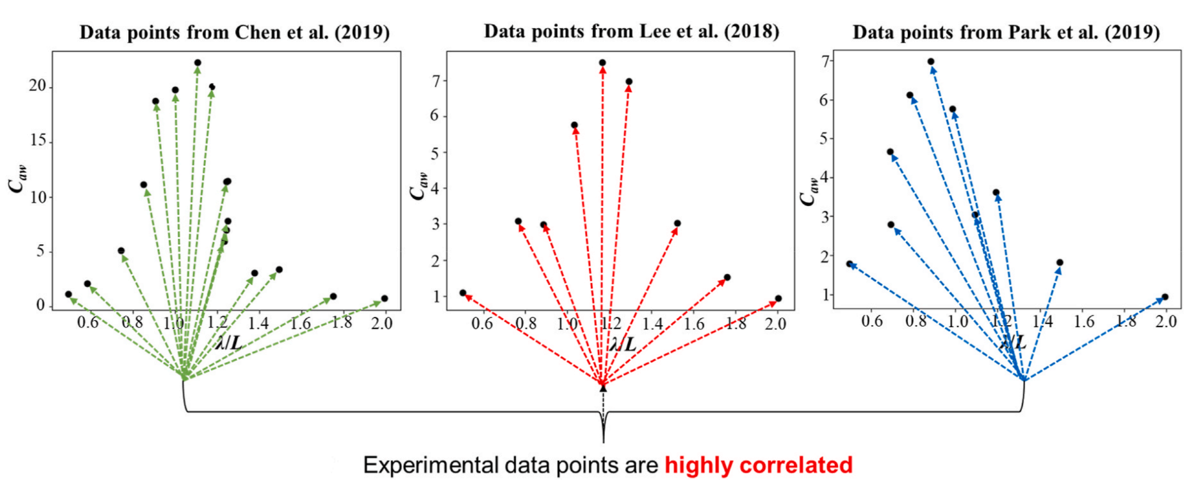

Fig. 5. Data points of experimental tests collected from public literature.

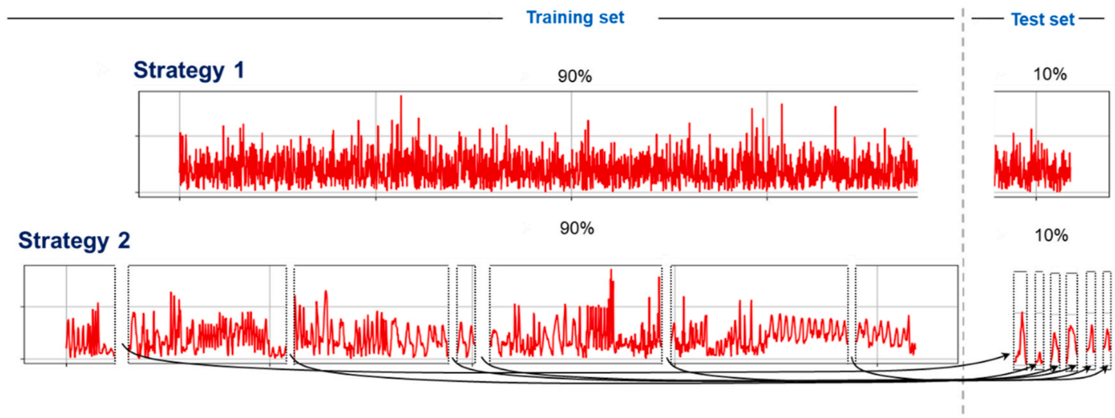

Fig. 6. Data partitioning strategies.

Where p_i is the predicted value; a_i denotes the actual value; n is the number of samples.

4. Overall results by different strategies 1&2

ANN and CTH models are utilized as comparisons to evaluate the performance of the GPR model. These models are chosen based on their established characteristics and application in wave resistance prediction. The CTH method refers to the semi-empirical formulas proposed by Lang and Mao [17].

4.1. Results using data partitioning strategy 1

For GPR modelling, we employ a four-fold cross validation to determine the hyperparameter settings, which is a commonly used method for machine learning method. By dividing the dataset into four subsets, each sample in the dataset serves as a validation set once. The model is then built based on the scores of the four different validation (unseen) datasets. This approach can help to avoid overfitting and improve the model's generalization capability. The Matern kernel [32] is chosen in this study from various covariance functions to calculate the kernel matrix.

50 samples, representing 25 % of the test set, are selected to provide detailed comparisons between predictions from the different models, as illustrated in Fig. 7. The results of whole test set are illustrated in Fig. 8. The RMSE values for the GPR, ANN, and CTH models are 0.95, 0.97, and 2.45, respectively. These results indicate that the semi-empirical formula method (CTH model) exhibits bigger uncertainty compared to the machine learning approaches (GPR and ANN). This result further suggests that, when modeling solely on the existing database, the predicted wave resistance coefficients will be accurate for ships whose ship types are included within the database. Moreover, as the database is continuously expanded with new entries, the model's predictive accuracy will further improve. This capacity for iterative update is an important advantage of machine learning–based approaches over semi-empirical formula methods.

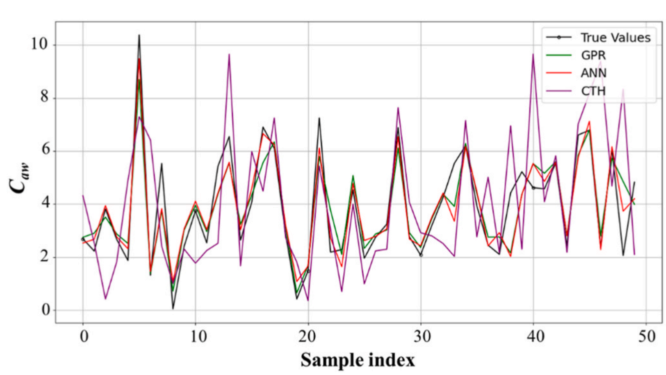

Fig. 7. The comparison between different methods and true values for 50 samples (25 % of test set) using data partitioning Strategy 1.

4.2. Results using data partitioning strategy 2

The strategy is to test the models' ability to predict resistance coefficients and plot reasonable resistance coefficient curves for different ship types and Froude numbers. Moreover, because the same ship type may be tested at different Froude numbers, it is possible during data selection to extract all test data corresponding to a particular ship type at a specific Froude number. In the extreme case where a ship type has only one set of experimental data, all those data may end up in the test set. Thus, this data splitting strategy can test the extrapolation capabilities of the two machine learning methods when dealing with ship types and Froude numbers that have not been observed. After several tests, the matern kernel is chosen for this case to calculate the covariance matrix.

The results on the test set obtained using Strategy 2 are presented in Figs. 9 and 10 and Table 3. It can be seen from the results that all three methods can capture the characteristic that the peak point of wave added resistance is around $\lambda/L = 1$, because the body's response to a wave field reaches its peak when the dimensions of wave are comparable to the body's dimensions. The CTH model achieves a "perfect" fit for the wave resistance coefficient curves of both the S175 and HSVA. This is because the CTH model uses similar datasets and statistical methods to determine its parameters [17]. Thus, for these two ship types, the CTH model can be regarded as an ideal model and serves as a benchmark for evaluating the other two machine learning models. For the S175 ship, the ANN model appears to overfit the data points, producing a strange curve shape. In contrast, although the GPR model exhibits slightly weaker predictive performance compared to the ANN, it generates a more reasonable curve. Furthermore, in the short-wave region, the GPR model successfully captures the correct trend, whereas the ANN model remains nearly constant. In estimating the HSVA wave resistance curve, the GPR model performs nearly as well as the ideal CTH model across long-wave, short-wave, and regions near $\lambda/\underline{L} = 1$. In addition to these two ship types, data for KVLCC are also incorporated into the CTH model; however, it cannot match the performance to GPR model, whereas the ANN model once again exhibits peculiar behavior near $\lambda/L = 1$. A possible explanation is that even for the same ship type, variations in experimental conditions can lead to different results. Thus, for these three ship types which have benchmarks, GPR model gives lower errors and produces a reasonable curve shape.

Aside from the S175, HSVA, and KVLCC, the CTH method does not include test data for other ship types considered in this study, thereby

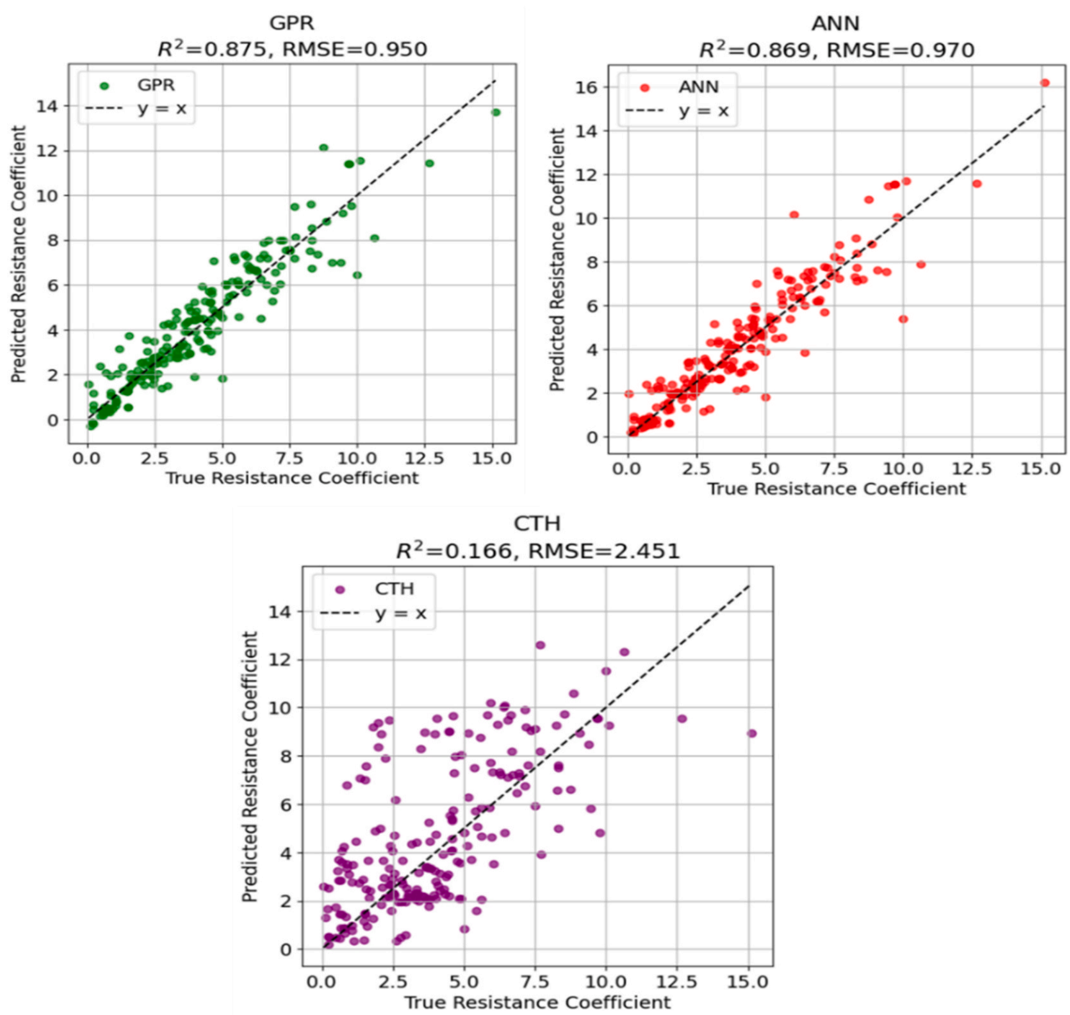

Fig. 8. Results using data partitioning Strategy 1.

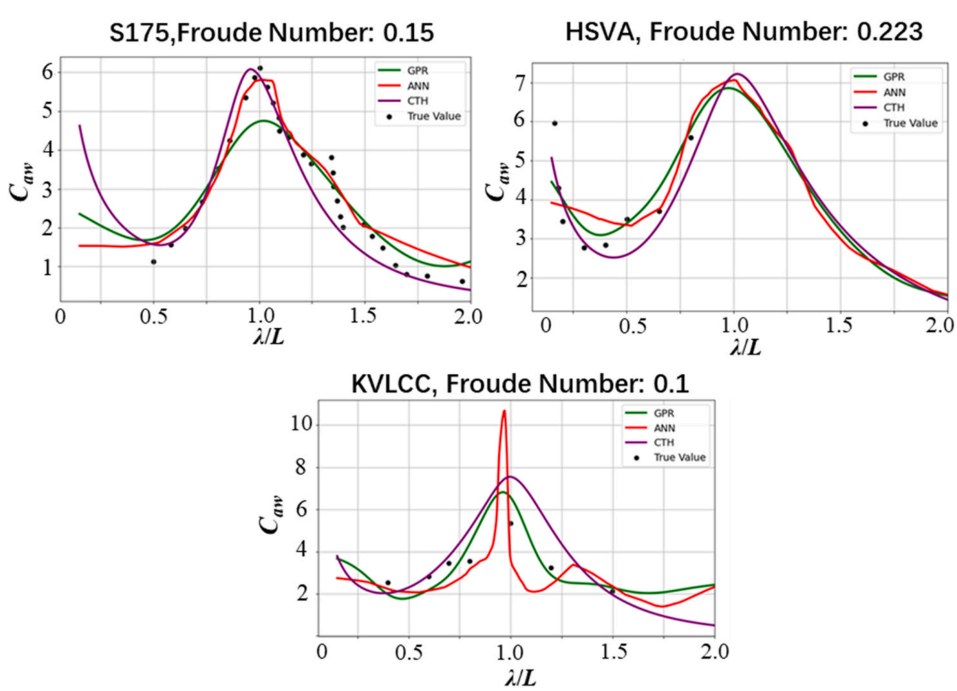

Fig. 9. Results for S175, HSVA and KVLCC using data partitioning Strategy 2.

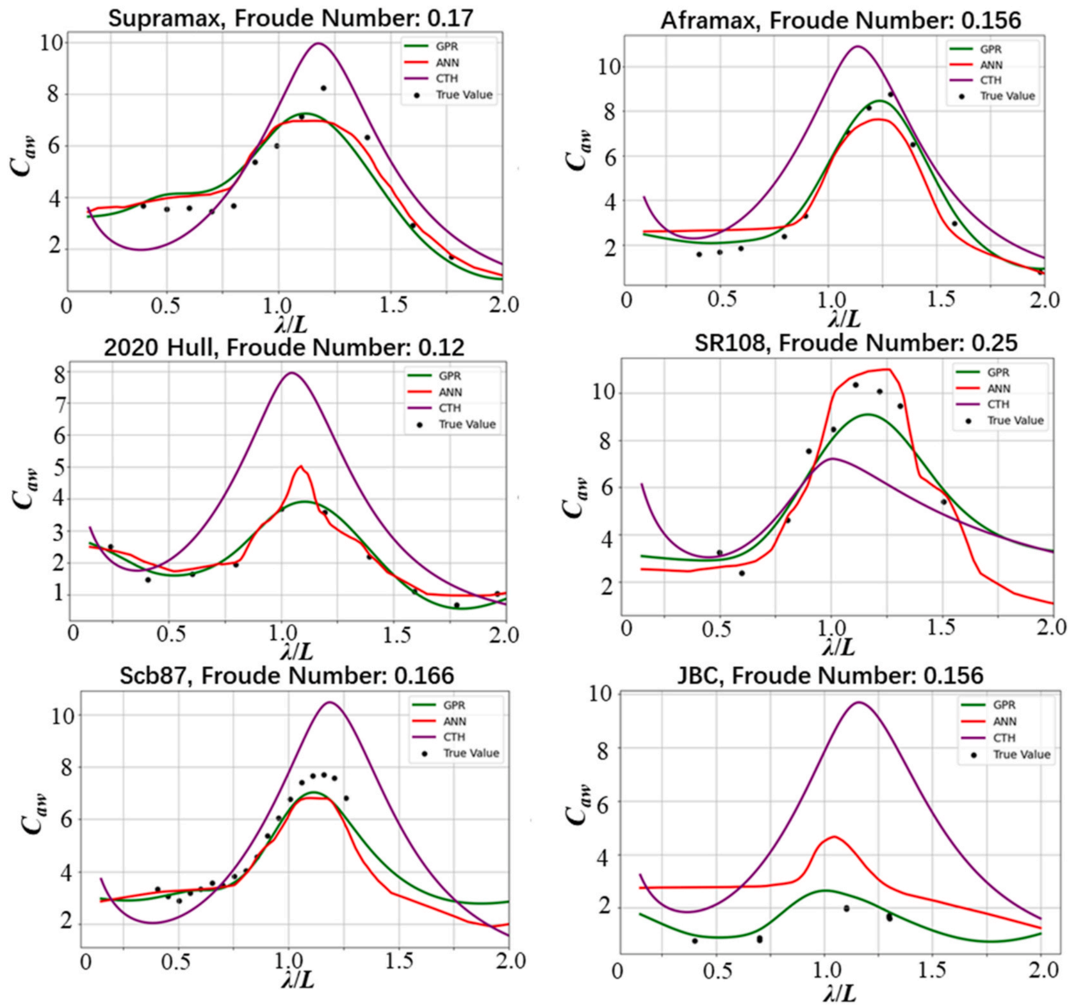

Fig. 10. Results for Supramax, Afamax, 2020 Hull, SR108, Scb87 and JBC using data partitioning Strategy 2.

Table 3
RMSE of different methods.

Model	F_n	GPR	ANN	CTH
S175	0.15	0.53	0.39	0.55
JBC	0.156	0.34	1.84	5.75
KVLCC	0.1	0.69	0.87	1.25
Supramax	0.17	0.71	0.61	1.25
HSVA	0.233	0.68	086	0.64
Aframax	0.156	0.39	0.69	2.07
2020 Hull	0.12	0.20	0.22	1.85
Scb87	0.166	0.45	0.54	1.48
SR108	0.25	0.88	0.82	2.21

naturally failing to predict their wave resistance coefficients, as shown in Fig. 10. Nevertheless, the wave resistance curves generated by the CTH model still provide a valuable reference for examining the overall trend.

Both the ANN and GPR models exhibit good predictive accuracy. However, the ANN model still fails in estimating the shape of the wave resistance curve, particularly in the short-wave region, where most of the ANN-generated curves appear as straight lines. In contrast, the GPR model often captures the correct variation trend. Moreover, when predicting the JBC wave resistance curve, only the GPR model produces acceptable results, while the other two methods fail. From the results above, the Gaussian process regression (GPR) model outperforms the artificial neural network (ANN) both in predictive accuracy and in plotting realistic curves for the wave resistance coefficients. Because the wave resistance coefficients exhibit an obvious correlation across consecutive wavelength/frequencies, the GPR model can capture this inherent dependency via its kernel function. In contrast, a standard ANN approach treats each sample as independent, which hinders its ability to reflect nature of wave resistance.

5. Application in ship performance prediction and weather impact

Due to environmental and economic considerations, the shipping industry has a growing demand for fuel consumption prediction under operational conditions. Given this background, reliable ship performance prediction in waves is crucial for ensuring optimal vessel operation.

In this section, the proposed GPR model is integrated into a ship performance model to calculate the fuel consumption during the ship's voyage. The results are then compared with full scale measurement data from a chemical tanker equipped with various sensors and devices to determine the deviation between the estimated and actual power. The weather impact on fuel consumption is also investigated in this section.

5.1. Case study full-scale measurements and metocean data

A 45000 DWT chemistry tanker with both self-propulsion test results and full-scale energy consumption measurements shown in Fig. 11 will be used for this study. This chemical tanker is equipped with various sensors and devices for data collection, with data being stored every second. The primary variables collected include propulsion system parameters (shaft power, torque, and RPM); navigational and operational information (latitude, longitude, course over ground, heading, draft at the bow and stern, speed over ground, and speed through water). Additionally, the ship is equipped with a data cleaning system that performs data cleaning on the raw measurements every 15 min. The self-propulsion model tests were carried out during her design stage to investigate the engine power needed for the vessel. Here it will serve as a baseline of ship power required for operation in calm water conditions. The main dimension of the ship is listed in Table 4.

Environmental information encountered by the ship during its voyage is needed for calculating the resistance. In this study, wind speed, wind direction, mean wave direction, wave period, and significant wave height are obtained from the European Centre for Medium-Range Weather Forecasts (ECMWF) reanalysis dataset, ERA5. Current velocity data were sourced from the Copernicus Marine Service. All data are based on a spatial resolution of $0.25 \times 0.25^{\circ}$, with a temporal resolution of 24 h for current velocity data and hourly for other data. The environmental data encountered by the vessel can be interpolated based on the ship's location and time to obtain the actual encountered conditions.

The entire dataset spans from 2014 to 2019. The raw measurements have been resampled at 15-min intervals and took the average of each interval, resulting in a total of 55,251 records. 5410 correspond to head sea conditions (in this study, relative wave angles between 0° and 10° are considered as head seas). Fig. 12 displays the ship's trajectories during this period, with the waypoints encountered by head seas highlighted. Fig. 13 illustrates the probability of distribution of various relative wave angles encountered during navigation. The dataset employed in this section encompasses diverse navigational routes, metocean conditions, and operational strategies. After removing outliers and observations recorded during non-sailing periods, the final dataset comprises 3936 observations.

Moreover, in addition to ship's principal dimensions and performance measurements, the shipowners provided baseline data from both model tests and sea trials—namely, the calm water resistance curve and wind resistance coefficients (Fig. 14). The wind resistance coefficient C_{AA} shown in Fig. 14 was measured in wind tunnel tests, while the calm water resistance and propulsive efficiency η was obtained from self-propulsion trials at the design draft across the operating speed range. The variables retained for subsequent modelling are shown in Table 5.

5.2. Comparison of a white box model with full-scale measurements

In a white box model, various ship resistances are determined in terms of ship speed, such as speed through water, metocean conditions (wind, wave, and current), etc. [17]. The engine shaft power is then estimated by effective propulsive power divided by various ship propulsion efficiencies [33]. Finally, fuel consumption is obtained through SFOC as in Eq. (3) [33]. In this study, we treat the GPR and semi-empirical models used for calculating fuel consumption as white box model based on prior knowledge (ship resistance and energy transfer), as shown in Fig. 15. Fig. 16 presents an example of fuel consumption estimations for head seas during the case ship's voyage, and

Table 4
Main parameters for model tests to determine engine power in calm water conditions self-propulsion tests for two loading conditions with model scale is 1:24.

Main parameters	Value
Length L [m]	176.0
Breadth B [m]	32.2
Designed draft T [m]	11.0
Maximum continuous power [kW]	8200
Deadweight DWT [tons]	46067
Wetted surface [m^2]	8166
Non-dimensional radius of gyration in yaw K_{yy} [$-$]	0.25
Block coefficient C_B [$-$]	0.80

Fig. 17 shows the distribution of estimation residuals, indicating that most estimates are underestimated. One potential cause of this underestimation could be the ship's extensive motions in rough seas, which may cause the propeller to emerge from the water, thereby reducing propulsion efficiency. Another possible reason is the ship's lack of regular maintenance in dry dock, leading to significant hull and propeller fouling. Furthermore, as mentioned before, the dataset spans a five-year period during which ship performance varied considerably; thus, these imprecise estimates are foreseeable. Moreover, we can assume that in actual operations, a ship's fuel consumption increases nonlinearly with increasing resistance.

5.3. A grey-box model for improving fuel consumption prediction

The uncertainties (the significant underestimation) observed in Figs. 16 and 17 may suggest that additional factors remain unaccounted when computing fuel consumption, as well as other nonlinear relationships within the ship propulsion system that require further investigation. Furthermore, since calm water resistance accounts for the largest proportion (as shown in Fig. 18), there is a high possibility that this discrepancy arises from the estimation of calm water resistance.

Because of bad prediction performance of white box model, a deep neural network (DNN), a black-box model, is introduced to model the residuals of the white box model, thereby forming a grey-box model [34, 35]. The grey-box model has two advantages for predicting fuel consumption: (1) it achieves higher predictive accuracy for most samples compared to the white box model, and (2) by incorporating prior knowledge, it has better extrapolation performance relative to the black-box model [36].

Similar grey box modelling approaches were investigated by various scholars in literature. For example, Leifsson et al. [37] first proposed serial and parallel grey box structures for ship fuel consumption prediction, showing that they outperform white box models in interpolation and black box models in extrapolation. Coraddu et al. [38] introduced a grey box method that reduces reliance on historical data. The authors conducted feature ranking analysis to check the physical plausibility of the model and ultimately applied the model as an online trim-optimization tool. Odendaal et al. [39] built a serial grey box model whose predictive accuracy and extrapolation capability exceeded those of black box models, although its performance still depended on the

Fig. 11. The ship (left) and her model test (right) for case study.

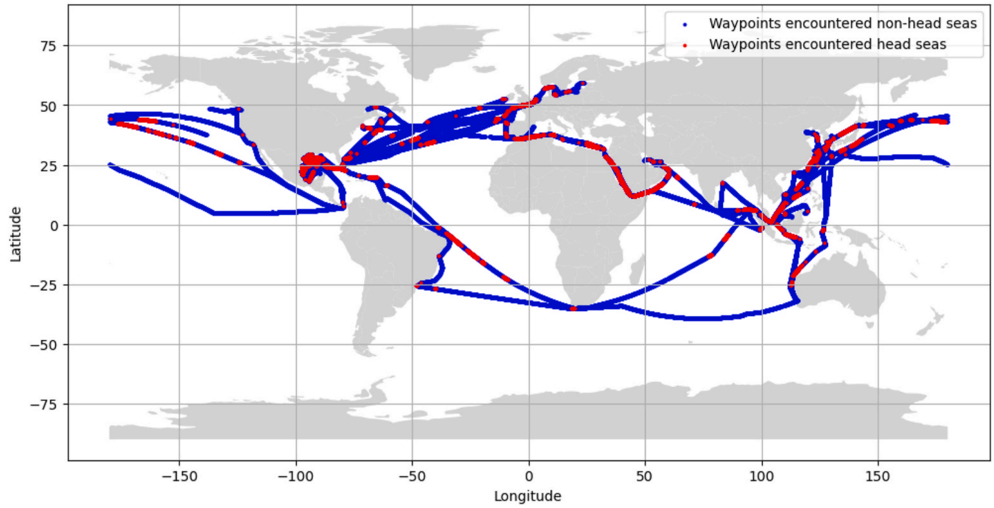

Fig. 12. Ship trajectories and waypoints encountered head seas from 2014 to 2019.

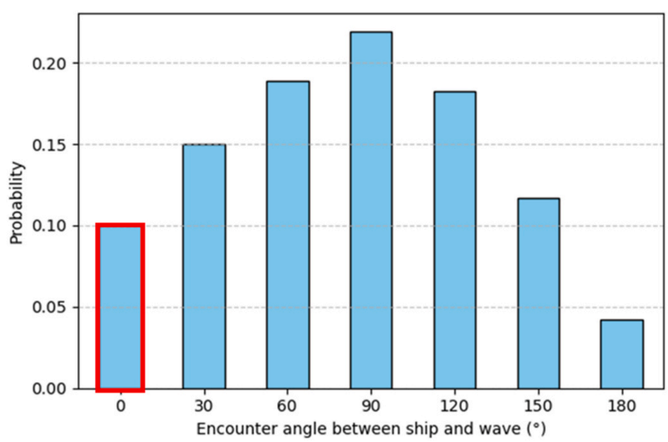

Fig. 13. The probability of different relative wave angles.

strength of dynamic input–output correlations in the white box component. Duan et al. (2025) introduced a methodological innovation in grey box modelling by designing a two-stage stacking framework that enhances predictive performance. By classifying operating conditions based on preliminary prediction errors, Fan et al. [36] employed Bayesian optimization to calculate optimal weights for each category and aggregate these weights for the final fuel consumption predictions.

In this study, the parallel grey box structure is established to integrate the developed GPR model for added wave resistance and time-related variables from monitoring data to model ship fuel consumption.

A purely black-box model for predicting total fuel consumption from ship speed and metocean conditions is not applicable for this study, as it cannot estimate wave resistance. Thus, a pure black-box fuel consumption prediction model will not be developed in the subsequent sections. The structure of the proposed grey-box fuel consumption model is illustrated in Fig. 19, which employs a parallel approach. The output of the grey-box model, FC_{pred_G}, is composed of the output from the white box model, FC_{pred_W}, plus the residual predicted by the black-box model, where the residual is computed as the difference between the measured fuel consumption FC_m and FC_{pred_W} [40].

Table 5
Variables for fuel consumption calculation.

Description	Data source
Engine shaft power [kW]	Full-scale measurements
Speed through water [kn]	Full-scale measurements
Heading [°]	Full-scale measurements
Mean draft [m]	Full-scale measurements
Specific fuel oil consumption (SFOC) [g/kWh]	Full-scale measurements
Significant wave height [m]	Hindcast
Mean wave period [s]	Hindcast
Wind speed [m/s]	Hindcast
Wind direction [°]	Hindcast

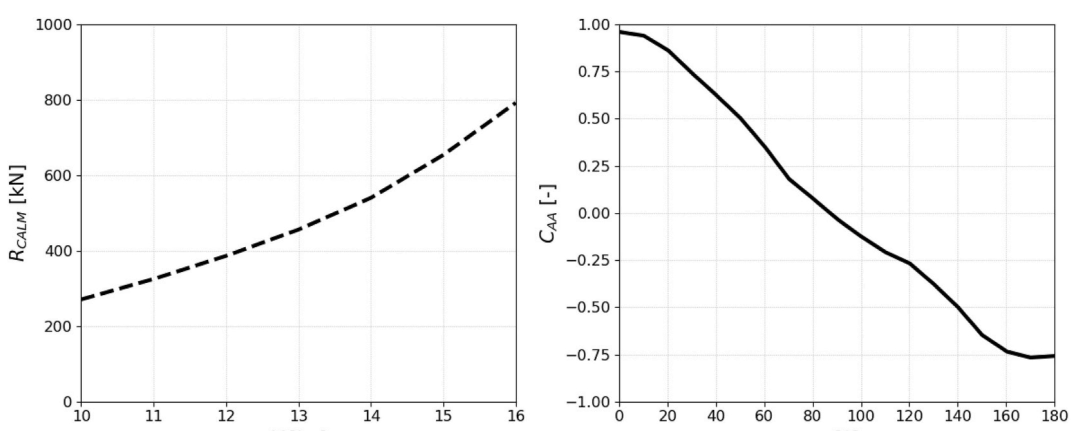

Fig. 14. Model test results of calm water resistance (left) and wind resistance coefficient (right).

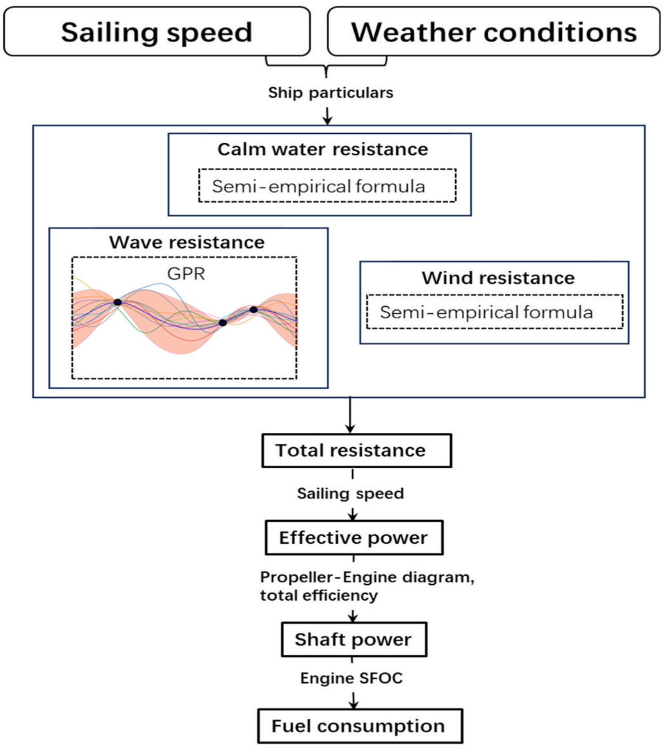

Fig. 15. Procedures for calculation fuel consumption.

Artificial neural networks (ANNs) simulate the operational patterns of human brain neurons by integrating many artificial neurons. In ANNs, the combination of each artificial neuron incorporating simple linear computations and nonlinear activation functions can approximate complex mapping relationships [41]. Compared to standard ANNs, deep neural networks (DNNs) have more hidden layers and thus greater learning capacity, making them more suitable for the large-sample, multi-feature regression tasks in this study. The modeling problem of DNN in this paper can be defined as follows, assuming for the i-th input data $\boldsymbol{x}_i$:

$$r_i = f_{DNN}(\boldsymbol{x}_i) + \rho_i \tag{21}$$

where ρ_i is the noise; $f_p(\cdot)$ represents the function of DNN model to predict residual r_i by the n-dimensional input $\boldsymbol{x}_i$. After entering the hidden layer in DNN, the output of the hidden layer h_j can be obtained:

$$h_j = f_a\left(\sum_{k=1}^{n} \omega_{jk} x_k - \theta_j\right) \tag{22}$$

where f_a is the activation function; x_k represents the k-th input variable' s value; ω_{jk} is the weight; θ_j is the threshold in this layer. The output of the hidden layer is then passed to the output layer, which produces the final prediction:

$$\hat{r} = g_a\left(\sum\nolimits_{j=1}^{l} \omega_j h_j - b_j\right) \tag{23}$$

where $\hat{r}$ is the predicted residual; $g_a(\cdot)$ serves as the output-layer activation; ω_j and b_j are the corresponding weights and bias terms. The prediction error (the difference between the true and predicted value) ε can be calculated as:

$$\varepsilon = \frac{1}{2}(r - \hat{r})^2 = \frac{1}{2}\left[r - g_a\left(\sum_{j=1}^{l} \omega_j f_a\left(\sum_{k=1}^{n} \omega_{jk} x_k - \theta_j\right) - b_j\right)\right]^2 \tag{24}$$

The error ε aggregates the individual output deviations of all neurons. During back-propagation, this error is sent from the output layer toward the input layer using the designed learning rate, and gradient descent method updates to the weights and biases iteratively shrink the network error until it satisfies the preset tolerance [41]. The hyper-parameters of DNN are determined using Bayesian optimization, and the results are shown in Table 6. The training set and test set are split in a 7:3 ratio, and all data has been standardized.

The prediction results of grey box model are presented in Fig. 20, with an R^2 of 0.95, representing a 38 % improvement over the white box model, and an RMSE of 45.65, indicating a 65 % reduction in error. This reveals a significant improvement from the white box model to the grey box model. The white box model ensures that predictions follow the basic physical principles, while its necessity to accommodate generic applications disadvantages it when applied to individual ship. In contrast, the significant improvement of the grey box model is because the black box component forces the model to transition from a generic framework to a ship-specific scope.

As previously discussed, the data set used in this study spans a large time range, and the ship's performance may change several times during this period. Thus, we consider including a time-related feature [42]. However, since the study focuses on head sea conditions, the dataset is not continuous in time. In addition, we prefer not to use "strong" features such as the speed at the previous time step ($v_{t\text{-}1}$). The reason is that using $v_{t\text{-}1}$ as a feature would limit the model's applicability, making it, for instance, unsuitable for weather routing. There are various

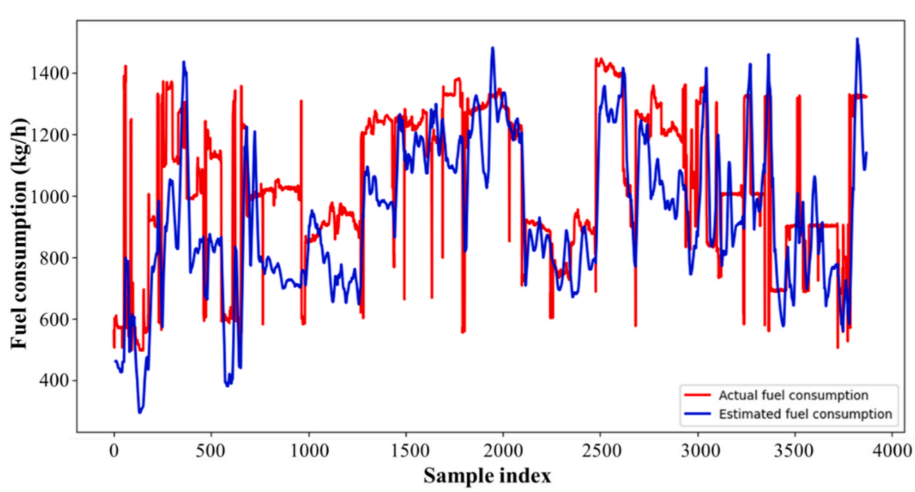

Fig. 16. Estimation of fuel consumption of studied chemical tanker.

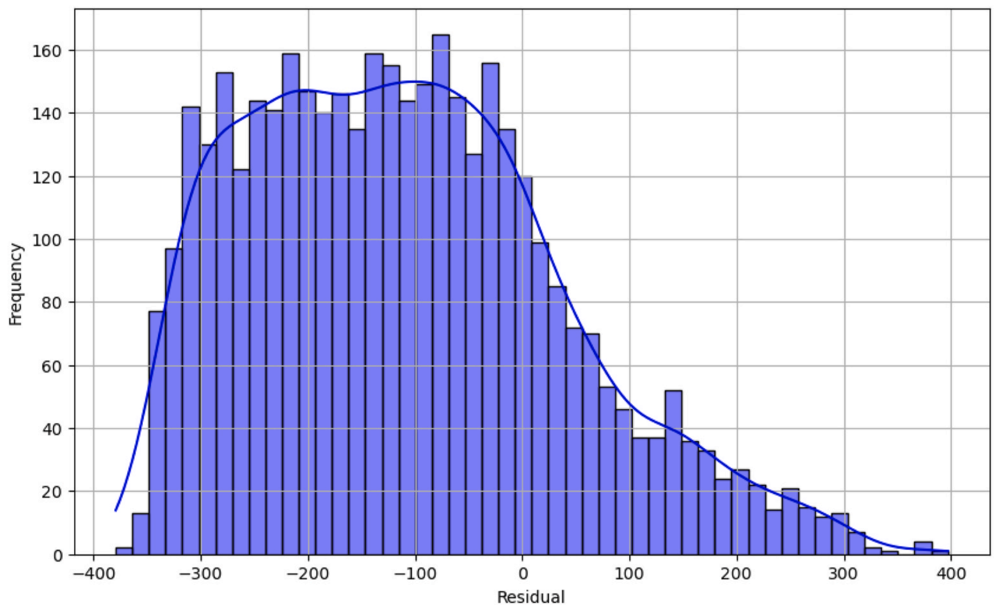

Fig. 17. Probability distribution of estimation residual.

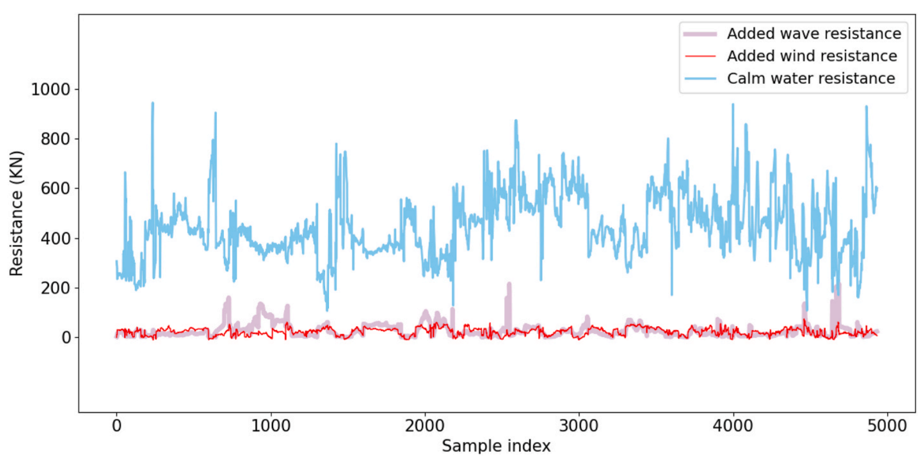

Fig. 18. Wave resistance, wind resistance, calm water resistance, and speed encountered during voyage.

alternative ways to incorporate temporal aspects, such as developing separate models for different voyages. Our goal is to enable the machine learning model to "understand" that ship performance becomes more similar when data points are closer in time. Therefore, we simply convert the time of each data point into a numeric timestamp and add it as an input feature. The timestamp-featured grey box model has further improvement on prediction.

By incorporating the timestamp feature, the grey-box model has achieved an additional performance boost, with R^2 increasing by 3 % and RMSE decreasing by 24 %, as illustrated in Fig. 21. This result indicates that even adding a "weak" feature, such as the timestamp, can improve model performance.

Although adding time-related features improves the model's prediction performance, it limits its applicability—for instance, making it unsuitable for weather routing [43]. This study proposes grey-box fuel consumption prediction models both with and without time features for different purposes. The model without time features can be directly applied to weather routing since the inputs to the grey-box model are either known (e.g., metocean information) or decision variables (e.g., speed and heading) in weather routing. While, the model that includes time features usually has better prediction performance, which is more suitable for ship performance monitoring and real-time operational optimization. In this study, the grey box model is used without a timetable to predict ship fuel consumption, and the results are shown in Fig. 22. We can see from Fig. 22 that the grey box model's predictions are reasonable, and the trend of fuel consumption varies with speed, draft, and wave height is consistent with real-world observations.

5.4. Weather impact on ship fuel consumption

The white box component of the grey box model can provide information, such as the various sources of resistance and the impact of weather on fuel consumption, for further applications. We calculate the distribution of wave-induced and wind-induced resistance when the case-study ship encountered head seas, as illustrated in Fig. 23, in which they show a clear positive correlation.

Weather-induced variations in resistance can lead to changes in a ship's fuel consumption. Figs. 24 and 25 illustrate the relationships between the ratio of fuel consumption due to weather impact to total fuel consumption, significant wave height, sailing speed, and draft under head sea conditions. As shown in these two figures, the weather-induced fuel consumption increases with rising wave height but

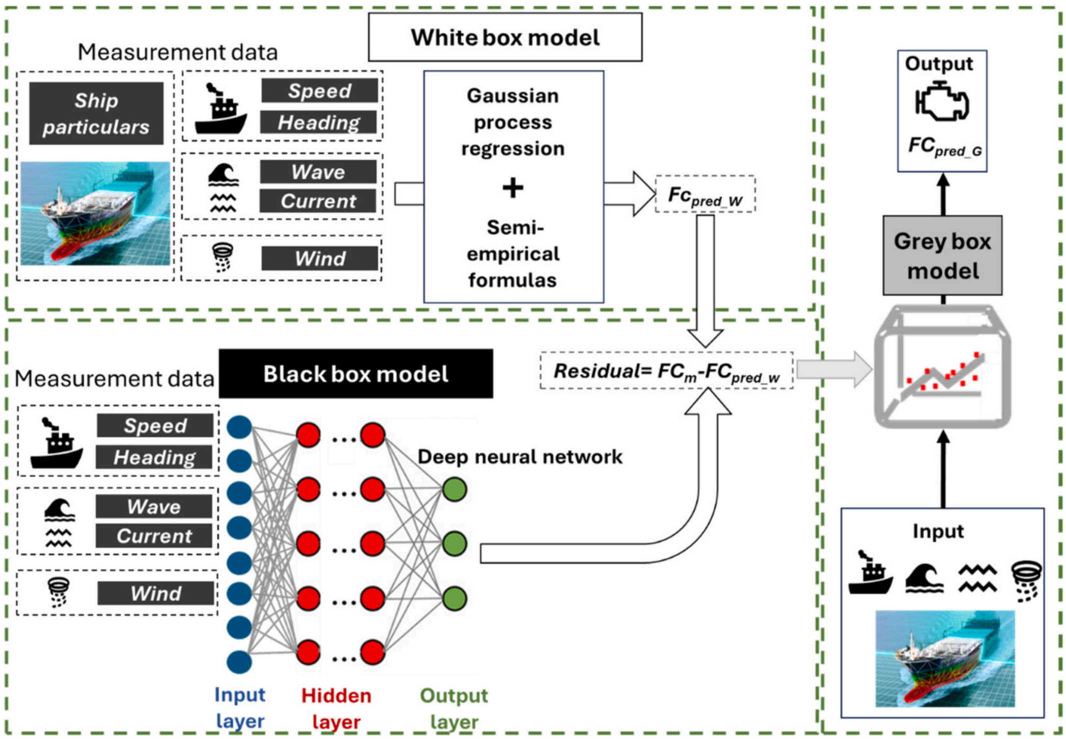

Fig. 19. Structure of grey box model.

Table 6
Hyperparameters for DNN.

Hyperparameters	Selection
Number of hidden layers	5
Number of hidden layer neurons	48
Activation function	ReLU
Learning rate	0.002

decreases as sailing speed increases. The former phenomenon is intuitive, since wave resistance generally grows with increasing wave height. The latter can be attributed to the fact that, at higher speeds, calm water resistance rises sharply, leading to a rapid increase in overall power demand. Thus, even though the additional resistance from wind and waves also increases, its relative proportion of the total resistance (or total fuel consumption) decreases.

As seen in Fig. 26, under head sea conditions, weather-induced fuel consumption can reach up to 39 % and averages around 8 %. These data demonstrate the impact of weather on fuel consumption, which is important for weather routing and for shipping companies seeking to reduce fuel costs.

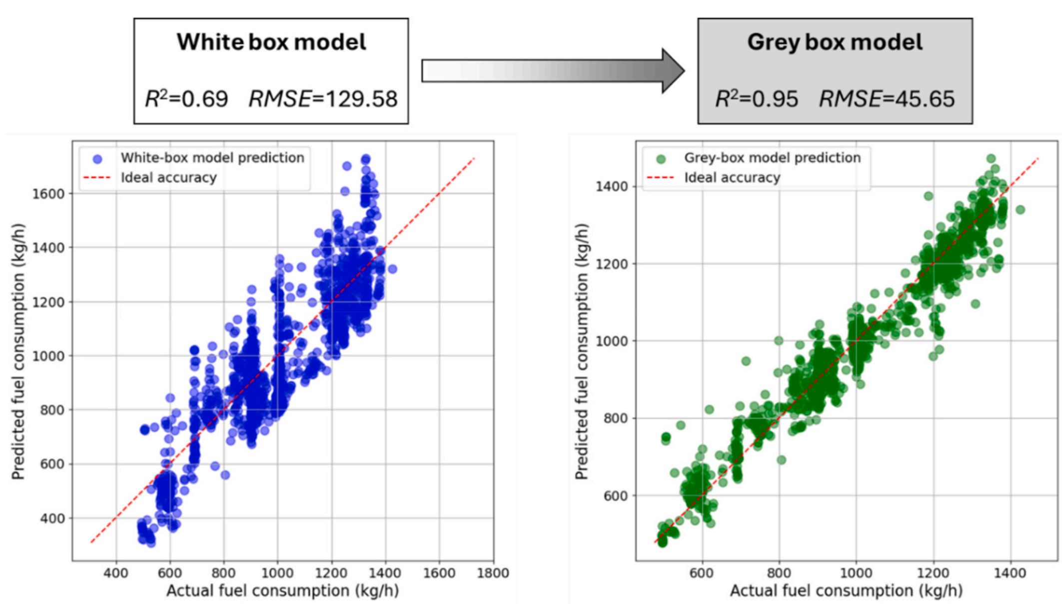

Fig. 20. Results of white and grey box model.

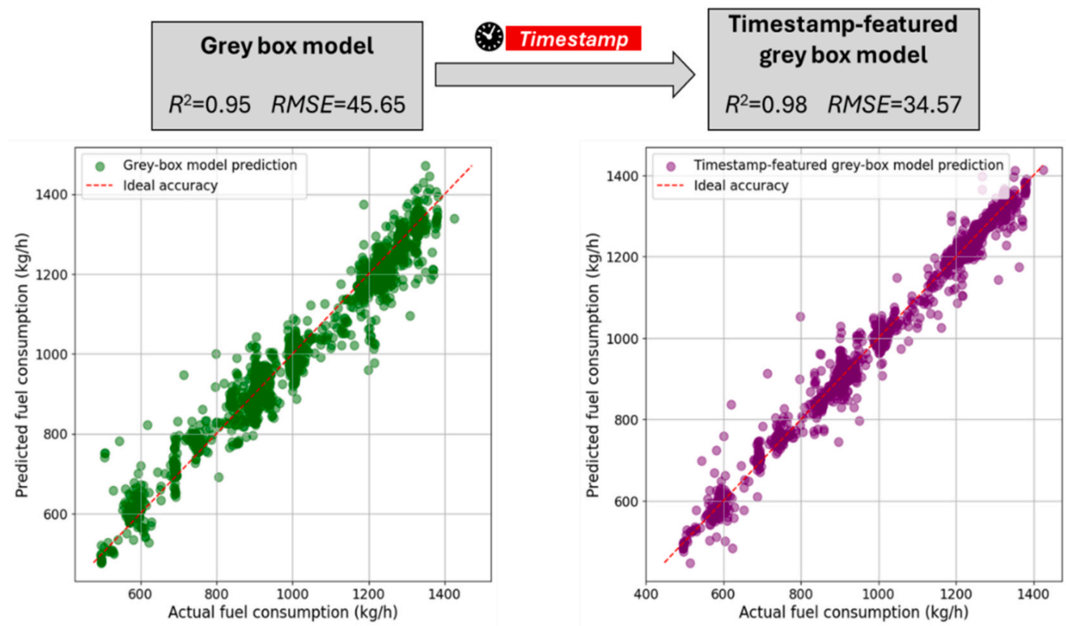

Fig. 21. Results of timestamp-featured grey box model.

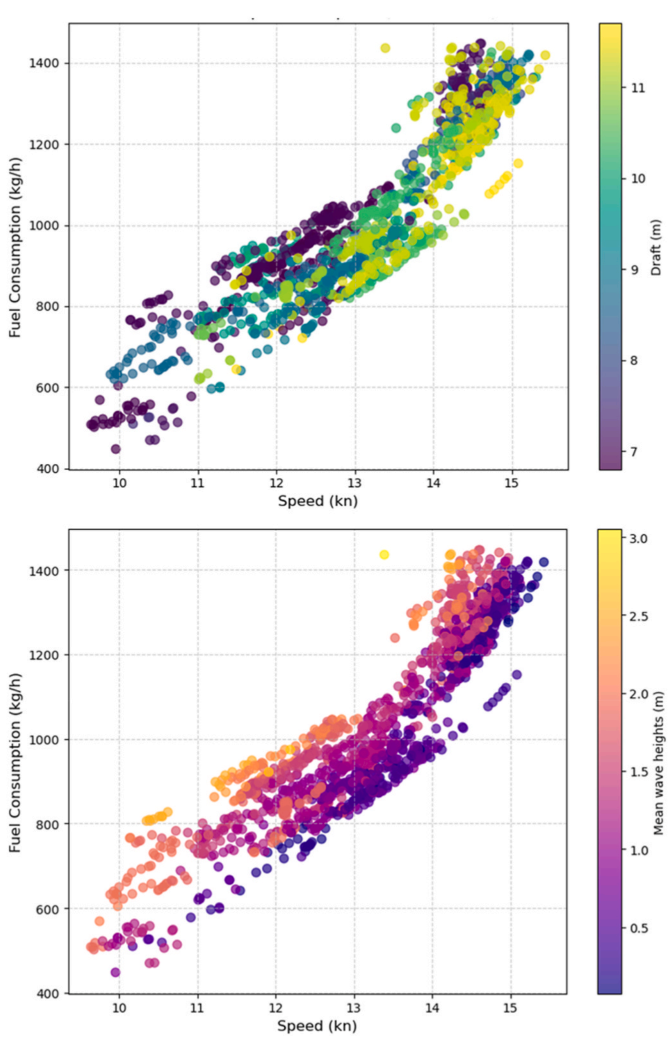

Fig. 22. The relationship between ship fuel consumption and external conditions (speed, draft, wave).

6. Conclusion

Predicting the added resistance of ships in head waves using publicly available experimental data has long been a challenging task. In this study, we addressed the correlations within these datasets and proposed a GPR model for predicting wave resistance coefficients across multiple ship types.

First, we introduce the dataset used for modeling, the model inputs and outputs, as well as the correlations among data points from the same experimental series. We then describe the working mechanism of the GPR model proposed in this paper. To validate the model's effectiveness, two different data splitting strategies are adopted. The simulation results show that, under a random splitting strategy, both the ANN and GPR machine learning methods outperform the semi-empirical method. For a customized dataset (Strategy 2), we evaluate all three methods in predicting wave resistance coefficient curves for different combinations of ship types and Froude numbers, and the findings are as follows:

- The semi-empirical approach can provide correct curve shapes but produces accurate estimates only for the ship types it considers.
- The ANN model achieves acceptable prediction errors for the wave resistance coefficients but fails to capture the curve shapes.
- The GPR method not only maintains sufficient accuracy but also captures the trends of wave resistance curves. In cases which have benchmarks (S175, HSVA, and KVLCC), its predictions and curve shapes are nearly on par with the "ideal" CTH model. Furthermore, the GPR model achieves satisfactory estimates even in situations (e.g., the JBC ship type) where both the ANN and CTH models fail.

Moreover, we incorporate the proposed GPR model into a white box model for estimating fuel consumption of a case study ship. The results indicate widespread underestimation, which lead us to introduce a grey box fuel consumption prediction model by integrating a DNN. The developed grey box model shows high accuracy for fuel consumption prediction. By applying the GPR model and the subsequent grey box model to the case-studied ship, the additional fuel consumption caused by weather conditions can be estimated, which may serve as a reference for ship energy saving and emission reduction.

It should be noted that the proposed GPR model sometimes performs incorrectly in the long-wavelength region. In future research, collecting

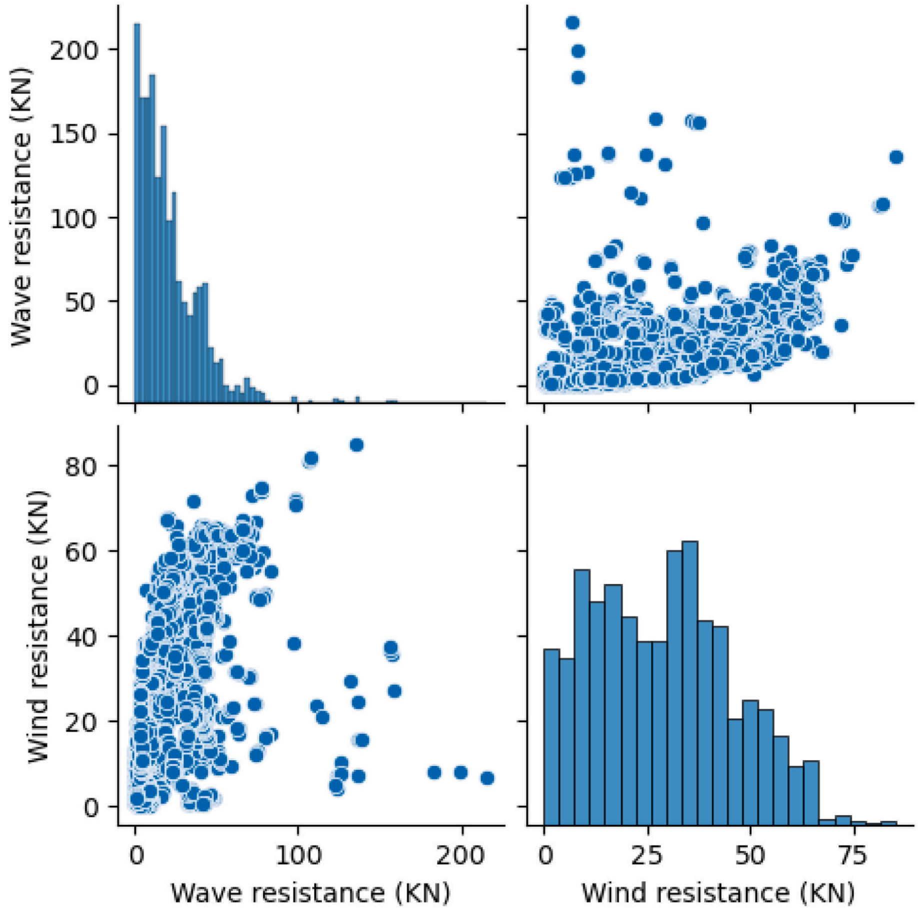

Fig. 23. Pairplot of wave resistance and wind resistance.

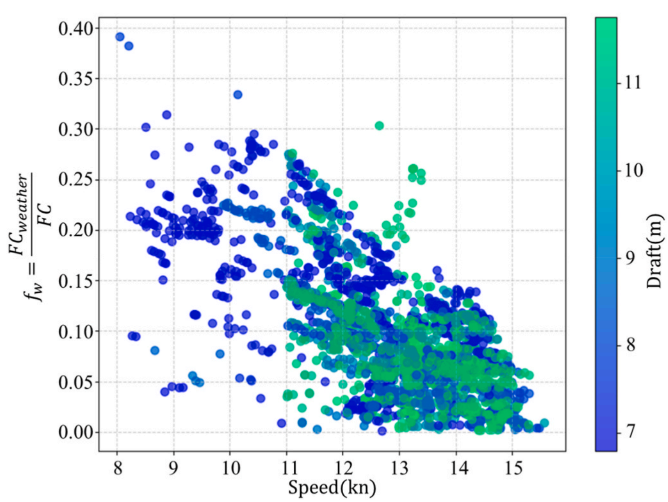

Fig. 24. Share of fuel consumption attributed to weather impact in terms of speed.

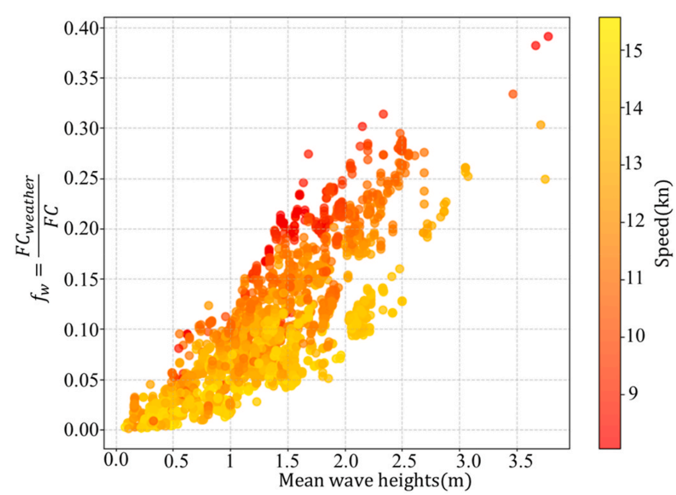

Fig. 25. Share of fuel consumption attributed to weather impact in terms of H_s.

more experimental data to enrich the model or incorporating the physical mechanisms of hull–wave interactions into the machine learning model could further enhance its generalization capability. Moreover, this study is currently limited to head seas. In future work, we will incorporate data collected at other wave encounter angles into the modeling framework to predict added wave resistance for arbitrary headings. To address the scarcity of data for wave encounter angles other than head seas, we will explore integrating physical mechanisms (e.g., semi-empirical formulations) within the machine learning approach. In addition, the influence of weather impact factors on the optimization of ship routing and speed will be investigated in future work.

CRediT authorship contribution statement

Chi Zhang: Writing – original draft, Visualization, Validation, Software, Methodology, Investigation, Formal analysis, Conceptualization.

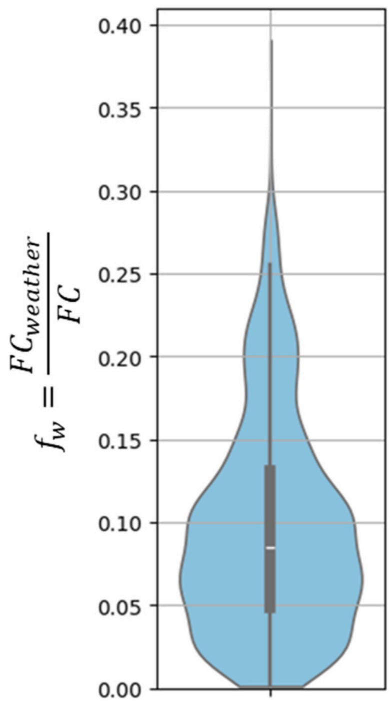

Fig. 26. The violin plot of statistical values of share of fuel consumption attributed to weather impact.

Daniel Vergara: Writing – original draft, Methodology, Data curation, Investigation, Formal analysis. **Mingyang Zhang:** Writing – review & editing, Supervision, Investigation, Formal analysis. **Tsoulakos Nikolaos:** Writing – review & editing, Data curation, Conceptualization. **Wengang Mao:** Writing – review & editing, Supervision, Project administration, Methodology, Funding acquisition, Conceptualization.

Declaration of competing interest

The authors declare that they have no known competing financial interests or personal relationships that could have appeared to influence the work reported in this paper.

Acknowledgments

The authors would like to acknowledge the funding from VINNOVA (Swedish Governmental Agency for Innovation Systems) [grant no. 2021-02768]; and Trafikverket (Swedish Transport Administration) [grant no. TrV 2023/98101]. The authors are also grateful to the ship owner for providing the full-scale measurement data.

Data availability

The authors do not have permission to share data.

References

[1] IMO. IMO strategy on reduction of GHG emissions from ships. 2023. 2023.
[2] DNV. Maritime forecast to 2050 - energy transition outlook 2023. 2023.
[3] DNV. Maritime forecast to 2050 - energy transition outlook 2024. 2024.
[4] Godet A, Wallner L, Panagakos G, Barfod M. Developing correction factors for weather's influence on the energy efficiency indicators of container ships using model-based machine learning. Ocean Coast Manag 2024;258:107390.
[5] Lang X, Wu D, Mao W. Comparison of supervised machine learning methods to predict ship propulsion power at sea. Ocean Eng 2022;245:110387.
[6] IMO. Draft guidelines for the calculation of the coefficient fw for decrease in ship speed in a representative sea condition. Mepc 64/4/38, vol. 2; 2012.
[7] Tillig F, Ringsberg J, Mao W, Ramne B. A generic energy systems model for efficient ship design and operation. Proc IME M J Eng Marit Environ 2017;231(2): 649–66.
[8] Kim K, Kim Y. Numerical study on added resistance of ships by using a time-domain Rankine panel method. Ocean Eng 2011;38(13):1357–67.
[9] Söding H, Shigunov V, Schellin T, Moctar O. A rankine panel method for added resistance of ships in waves. J Offshore Mech Arctic Eng 2014;136(3):031601.
[10] Liu S, Papanikolaou A. Fast approach to the estimation of the added resistance of ships in head waves. Ocean Eng 2016;112:211–25.
[11] Kim Y, Esmailian E, Steen S. A meta-model for added resistance in waves. Ocean Eng 2022;266:112749.
[12] Lee C, Park S, Yu J, Choi J, Lee I. Effects of diffraction in regular head waves on added resistance and wake using CFD. Int J Nav Archit Ocean Eng 2019;11(2): 736–49.
[13] Kim T, Yoo S, Kim H. Estimation of added resistance of an LNG carrier in oblique waves. Ocean Eng 2021;231:109068.
[14] Chen J, Duan W, Ma S, Liao K. Time-domain TEBEM method for mean drift force and moment of ships with forward speed under the oblique seas. J Mar Sci Technol 2021:1–13.
[15] Fujii H, Takahashi T. Experimental study on the resistance increase of a large full ship in regular oblique waves. J Soc Nav Archit Jpn 1975;1975(137):132–7.
[16] Liu S, Papanikolaou A. Regression analysis of experimental data for added resistance in waves of arbitrary heading and development of a semi-empirical formula. Ocean Eng 2020;206:107357.
[17] Lang X, Mao W. A semi-empirical model for ship speed loss prediction at head sea and its validation by full-scale measurements. Ocean Eng 2020;209:107494.
[18] Cepowski T. The prediction of ship added resistance at the preliminary design stage by the use of an artificial neural network. Ocean Eng 2020;195:106657.
[19] Duan W, Yang K, Huang L, Jing Y, Ma S. A DFN-based method for fast prediction of ships' added resistance in heading waves. Ocean Eng 2022;245:110484.
[20] Cepowski T. The use of a set of artificial neural networks to predict added resistance in head waves at the parametric ship design stage. Ocean Eng 2023;281: 114744.
[21] Sun Q, Zhang M, Zhou L, Garme K, Burman M. A machine learning-based method for prediction of ship performance in ice: part I. ice resistance. Mar Struct 2022;83: 103181.
[22] Rasmussen CE, Williams CKI. Gaussian processes for machine learning. Cambridge, Massachusetts: MIT Press; 2006.
[23] ITTC. Resistance uncertainty analysis example for resistance test. Recommended procedures 2002;7. 5-02-02-02.
[24] ISO. BS ISO 15016:2015 - annex B: beaufort scale for wind velocity. 2015.
[25] Faltinsen O. Prediction of resistance and propulsion of a ship in a seaway. 13th symposium on naval hydrodynamics, Tokyo. 1980. p. 505–29.
[26] Jinkine V, Ferdinande V. A method for predicting the added resistance of fast cargo ships in head waves. Int Shipbuild Prog 1974;21(238):149–67.
[27] Tsujimoto M, Shibata K, Kuroda M, Takagi K. A practical correction method for added resistance in waves. J Jpn Soc Nav Archit Ocean Eng 2008;8:177–84.
[28] Lang X, Mao W. A practical speed loss prediction model at arbitrary wave heading for ship voyage optimization. J Mar Sci Appl 2021;20(3):410–25.
[29] Chen X, Ren Y, Xiao H, Cai X, Zhu R. A MDHOBEM energy radiated method to evaluate added wave resistance of ship. International ocean and polar engineering conference (ISOPE). ISOPE; 2019. p. 19–684. I.
[30] Lee J, Kim S, Lee S, Kang D, Lee J. Prediction of added resistance using genetic programming. Ocean Eng 2018;153:104–11.
[31] Park D, Lee J, Jung Y, Lee J, Kim Y, Gerhardt F. Experimental and numerical studies on added resistance of ship in oblique sea conditions. Ocean Eng 2019;186: 106070.
[32] Elshafei B, Popov A, Giddings D. Enhanced offshore wind resource assessment using hybrid data fusion and numerical models. Energy 2024;310:133208.
[33] Wang H, Lang X, Mao W, Zhang D, Storhaug G. Effectiveness of 2D optimization algorithms considering voluntary speed reduction under uncertain metocean conditions. Ocean Eng 2022;200:107063.
[34] Luo X, Yan R, Xu L, Wang S. Accuracy and applicability of ship's fuel consumption prediction models: a comprehensive comparative analysis. Energy 2024;310: 133187.
[35] Karatuğ Ç, Tadros M, Ventura M, Guedes Soares C. Decision support system for ship energy efficiency management based on an optimization model. Energy 2024;292: 130318.
[36] Fan A, Wang Y, Yang L, Yang Z, Hu Z. A novel grey box model for ship fuel consumption prediction adapted to complex navigating conditions. Energy 2025; 315:134436.
[37] Leifsson L, Sævarsdóttir H, Sigurðsson S, Vésteinsson A. Grey-box modeling of an ocean vessel for operational optimization. Simulat Model Pract Theor 2008;16(8): 923–32.
[38] Coraddu A, Oneto L, Baldi F, Anguita D. Vessels fuel consumption forecast and trim optimisation: a data analytics perspective. Ocean Eng 2017;130:351–70.
[39] Odendaal K, Alkemade A, Kana A. Enhancing early-stage energy consumption predictions using dynamic operational voyage data: a grey-box modelling investigation. Int J Nav Archit Ocean Eng 2023;15:100484.
[40] Ruan Z, Huang L, Li D, Ma R, Wang K, Zhang R, Zhao H, Wu J, Li X. A novel dual-stage grey-box stacking method for significantly improving the extrapolation performance of ship fuel consumption prediction models. Energy 2025:134927.

[41] Zhang C, Zhang D, Zhang M, Mao W. Data-driven ship energy efficiency analysis and optimization model for route planning in ice-covered Arctic waters. Ocean Eng 2019;186:106071.
[42] Wang K, Liu X, Guo X, Wang J, Wang Z, Huang L. A novel high-precision and self-adaptive prediction method for ship energy consumption based on the multi-model fusion approach. Energy 2024;310:133265.
[43] Zhang C, Zhang D, Zhang M, Zhang J, Mao W. A three-dimensional ant colony algorithm for multi-objective ice routing of a ship in the Arctic area. Ocean Eng 2022;266:113241.